

PCCP

Accepted Manuscript



This is an *Accepted Manuscript*, which has been through the Royal Society of Chemistry peer review process and has been accepted for publication.

Accepted Manuscripts are published online shortly after acceptance, before technical editing, formatting and proof reading. Using this free service, authors can make their results available to the community, in citable form, before we publish the edited article. We will replace this *Accepted Manuscript* with the edited and formatted *Advance Article* as soon as it is available.

You can find more information about *Accepted Manuscripts* in the [Information for Authors](#).

Please note that technical editing may introduce minor changes to the text and/or graphics, which may alter content. The journal's standard [Terms & Conditions](#) and the [Ethical guidelines](#) still apply. In no event shall the Royal Society of Chemistry be held responsible for any errors or omissions in this *Accepted Manuscript* or any consequences arising from the use of any information it contains.

Cite this: DOI: 10.1039/c0xx00000x

www.rsc.org/xxxxxx

ARTICLE TYPE

***In Situ* back-side illumination fluorescence XAFS (BI-FXAFS) studies on platinum nanoparticles deposited on a HOPG surface as a model fuel cell: A new approach to the Pt-HOPG electrode/electrolyte interface**

Hiromitsu Uehara,^a Yohei Uemura,^a Takafumi Ogawa,^a Kentaro Kono,^a Ryoichi Ueno,^a Yasuhiro Niwa,^b Hiroaki Nitani,^b Hitoshi Abe,^b Satoru Takakusagi,^a Masaharu Nomura,^b Yasuhiro Iwasawa^c and Kiyotaka Asakura^{*a}

Received (in XXX, XXX) Xth XXXXXXXXX 20XX, Accepted Xth XXXXXXXXX 20XX

DOI: 10.1039/b000000x

We measured the *in situ* polarization-dependent X-ray absorption fine structure of platinum nanoparticles (PtNPs) deposited on a flat highly oriented pyrolytic graphite (HOPG) substrate under electrochemical conditions using a back-side illumination method. In this method, the thin HOPG substrate with PtNPs deposited on one side was used as a window for incident and fluorescent X-rays, as well as an electrode. A bent crystal Laue analyzer (BCLA) was applied to the extraction of the Pt L_α fluorescent X-ray signals from strong scattered X-rays. Pt L₃ edge XAFS spectra were observed at various electrode potentials and polarization directions.

Introduction

Polymer electrolyte fuel cells (PEFCs) are considered a next-generation clean energy source with high energy conversion efficiency and power density at low temperatures. Platinum (Pt) is widely used as an electrocatalyst in PEFCs because of its high catalytic activity and durability for the hydrogen oxidation reaction, oxygen reduction reaction and methanol oxidation reaction. Thus, the interaction among platinum nanoparticles (PtNPs), carbon supports and polymer electrolyte in membrane electrode assemblies have been studied extensively.¹⁻⁹ The durability of PEFCs strongly depends on the degradation process of electrocatalysts at electrode/electrolyte interface.¹⁰⁻¹⁴ However, the stabilizing interaction of active nanoparticles with the carbon support at an atomic scale remains unclear. Understanding this chemical interaction, particularly under electrochemical conditions, will allow new fuel cell electrocatalysts with a long life time and high performance to be designed.

X-ray absorption fine structure (XAFS) is an appropriate technique to investigate the interactions around X-ray-absorbing atoms in PEFCs under *in situ* conditions.¹⁵⁻¹⁸ Conventional XAFS usually uses powder samples, and bond distances in all directions are averaged to give a one-dimensional radial function. If an atomically flat surface is used, where the angle (θ_i) between the X-ray polarization direction and bonding direction can be well defined, we can achieve three-dimensional structure analysis using the polarization dependence of XAFS oscillations to provide detailed structural information about electrocatalysts.¹⁹ However, the surface area of flat substrates such as highly oriented pyrolytic graphite (HOPG) is very small, so the amount

of one monolayer Pt deposited on the HOPG is limited to less than about 10¹⁵ atom·cm⁻². We developed the polarization-dependent total reflection fluorescence XAFS (PTRF-XAFS) method to determine the three-dimensional structure of metal species dispersed on a flat surface such as single crystal oxides.¹⁹ Under total reflection conditions where an X-ray is introduced to a surface at a grazing angle of around 5-10 mrad, the X-ray can only penetrate into the material by 1-2 nm. We previously examined 10¹³ atom·cm⁻² Ni species dispersed on TiO₂(110) using PTRF-XAFS.²⁰ Total reflection fluorescence XAFS has also been applied to electrode/electrolyte interfaces.²¹⁻²⁶ As a model carbon electrode, HOPG is an ideal candidate for PTRF-XAFS. However, we have encountered several problems when attempting to apply PTRF-XAFS to Pt electrocatalysts on HOPG substrates under working conditions. First, the critical angle of total reflection is too small (2.62 mrad at Pt L₃ edge, $\lambda = 0.107$ nm or $E = 11.6$ keV) because critical angle of the total reflection is proportional to electron density, which is small for HOPG. Secondly, it is difficult to obtain an atomically flat HOPG surface with cm-size necessary for total reflection. AFM indicated HOPG itself has an atomically flat surface in the nm- μ m domain scale, although the flat domain is not large enough to give good total reflection as mentioned later. The third problem is the thin electrolyte layer. When one tries to carry out *in situ* PTRF-XAFS under electrochemical conditions, a thin electrolyte layer between the sample surface and X-ray window, as shown in Fig. 1a and b, is necessary to decrease the absorption and scattering of electrolyte because the grazing angle of the incident X-ray is almost parallel to the surface, which means the X-ray has a long distance to travel through the electrolyte. However, a thin electrolyte layer prevents effective mass transport to the electrode surface. When the reaction occurs, the sample must be moved

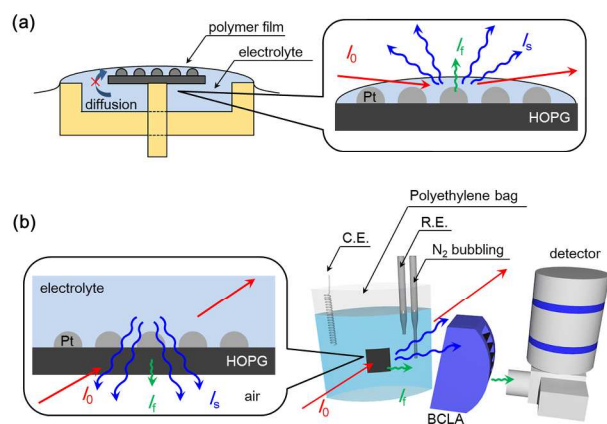


Fig. 1 Schematic illustrations of the experimental set up. (a) PTRF-XAFS configuration under electrochemical conditions. (b) Back-side illumination (BI) configuration with a BCLA used in this study. C.E. and R.E. are counter and reference electrodes, respectively. Incident X-ray (I_0), scattering X-ray (I_s) and fluorescent X-ray (I_f) are shown in red straight, blue long wavy and green short wavy arrows, respectively.

away from the window to produce a thick electrolyte layer to ensure material transfer and electrochemical equilibrium.

We have solved these problems by developing a different type of polarization dependent fluorescence XAFS. The high transparency of HOPG (attenuation length is 3.2 mm at $\lambda = 0.107$ nm) markedly reduces the scattering from bulk HOPG, so it might be possible to detect surface species without total reflection conditions. Moreover, if a thin HOPG layer can be used as an X-ray window and electrode at the same time, as shown in Fig. 1b, the absorption of the solvent can be neglected, which may allow the system to contain a thick enough electrolyte layer. HOPG has a layered structure with large tensile strength,²⁷ and thin graphite layers are readily peeled off by adhesive tape.²⁸ Pt was deposited on the surface of HOPG exposed to electrolyte, while the back-side of HOPG without Pt and solvent contact was exposed to X-rays. The developed method is called back-side illumination fluorescence XAFS (BI-FXAFS). The back-side illumination configuration has already been utilized in the field of X-ray spectroscopies such as XAS²⁹, XES³⁰ and XPS^{31,32}. However, in this configuration, the X-ray scattering from the electrolyte hinders the X-ray fluorescence measurements of small amount of surface species with low density (about 1×10^{14} atoms cm^{-2}). The tail of elastic scattering from the electrolyte was too large to observe the fluorescence signals of the target element in the presence of solvent. To solve this problem, we used a high-acceptance-solid-angle monochromator, a bent crystal Laue analyzer (BCLA), which was developed by Bunker and co-workers.³³⁻³⁵ In this paper, we report that the XAFS signals of a small amount of PtNPs ($\sim 1 \times 10^{14}$ atom $\cdot \text{cm}^{-2}$) deposited on an HOPG substrate can be detected in the presence of electrolyte in electrochemical equilibrium using a BI configuration and BCLA. We determine the potential and polarization dependence of the structure and electronic state of Pt nanoclusters on an HOPG surface.

35 Experimental

Materials and Sample Preparation

All reagents were purchased and used without further purification. We used two types of HOPG. One was ZYA (mosaic spread (MS) = $0.4 \pm 0.1^\circ$) and the other was ZYH (MS = $3.5 \pm 1.5^\circ$). Note that both ZYH and ZYA grades have atomically flat surface, giving good AFM or STM images. For PTRF-XAFS we need large mirror surface, we used ZYA grade HOPG ($10 \times 10 \times 1$ mm). For the BI-FXAFS measurements, a very thin HOPG flake was necessary, which was prepared by the peel-off method using adhesive tape. Since ZYH grade could provide a large and durable thin flake but the ZYA grade could not, we used ZYH grade HOPG for BI-FXAFS measurements. The adhesive tape was then removed from the HOPG flake by immersion in diethyl ether for 1 h. The resulting HOPG flake had dimensions of 10×10 mm and was a few tens of μm thick. The thin HOPG flake was then washed by immersion in fresh diethyl ether twice and stored in the solvent until use.

Dodecanethiol-protected PtNPs were synthesized according to the literature.³⁶ We describe the preparation method briefly here. Sodium acetate (620 mg, 7.6 mmol) and potassium tetrachloroplatinate (66 mg, 0.16 mmol) were dissolved in 1,2-ethanediol (50 mL) and heated at 353 K for 30 min. The solution was then cooled to room temperature and poured into toluene (50 mL) containing dodecanethiol (30.4 mg, 0.15 mmol) under vigorous stirring. The PtNP-containing toluene phase was separated, washed three times with deionized water and dried with Na_2SO_4 . Half of the solution was stored separately and used for XAFS measurements (denoted "as-syn."). Toluene was removed from the other half by a rotary evaporation. The residue was washed with copious amount of ethanol, and then dried in *vacuo*. The dodecanethiol-coated PtNPs were redispersed in hexane (1.5×10^{-2} wt%) and deposited on HOPG by spin coating (3000 rpm, 1 min). After the spin coating, dodecanethiol layers were removed by electrochemical oxidation-reduction cycles (ORC) treatment in 0.1 M HClO_4 aqueous solution. (The sample was denoted as thin PtNPs/HOPG.) The electrolyte solution was deaerated by bubbling pure N_2 gas through it for 30 min prior to electrochemical measurements. Pt wire was used as the counter electrode. A reversible hydrogen electrode (RHE) or Ag/AgCl (saturated NaCl) was used as the reference electrode. All electrode potentials were reported in respect to RHE (0.00 V vs H^+/H_2) as the reference. In XAFS experiments, HOPG with PtNPs was used as an X-ray window fixed to a 5mm^2 hole on the side of a polyethylene bag with glue as shown in Fig. 1b. The bag was filled with electrolyte and equipped with reference and counter electrodes. The outer surface of HOPG was then coated with transparent nail polish to prevent water leakage (Fig. 1b). Cu wire ($\phi = 0.3$ mm) was also fixed at the air side as a lead wire. We confirmed experimentally that the metallic Pt wire used as a counter electrode did not affect the spectral measurements because it was located far from the emission source point and covered with Pb sheets.

X-ray photoelectron spectra (XPS) were measured by a JEOL JPS-9010MC, Japan) spectrometer. Transmission electron microscope (TEM) images of the PtNPs were obtained by a JEOL JEM-2100F TEM. The surface morphology of PtNPs coated on HOPG was analyzed by AFM (Cypher; Asylum Research, CA, USA). XAFS measurements were carried out at the BL9A beam line of the Photon Factory at the Institute of Material

Structure Science (KEK-IMMS-PF), which was operated at 2.5 GeV and 450 mA. X-rays were monochromatized using a Si(111) double-crystal monochromator. Fluorescence X-rays were detected by a 19-element pure Ge solid-state detector (SSD) (GL0110S; Canberra, CT, USA). A Ge fluorescence filter was used to reject elastic scattering together with a Soller slit. Note that a Zn filter, which is usually recommended for Pt L₃ edge fluorescence measurements, was not able to be used because Zn K_β (9.572 keV) overlaps with Pt L_α (9.442 keV).

For the *in situ* measurements in the presence of electrolyte, the fluorescence signal was extracted from scattered X-rays using a BCLA (0095; FMB Oxford, UK). A pure Ge SSD or a pixel-array detector (PILATUS 100K; Dectris, Switzerland) was placed behind the BCLA to monitor the fluorescence signal. The BCLA and the detector were completely covered with Pb plates to remove stray X-rays scattered without passing through the BCLA. XAFS analysis was performed using a REX 2000 (Rigaku Co.) analysis program package for background subtraction.^{37, 38}

Results and Discussion

Surface Morphology and Electrochemical Properties of PtNPs on HOPG

Fig. 2a and b show AFM images of an HOPG surface partially covered with PtNPs. The dodecanethiol-protected PtNPs

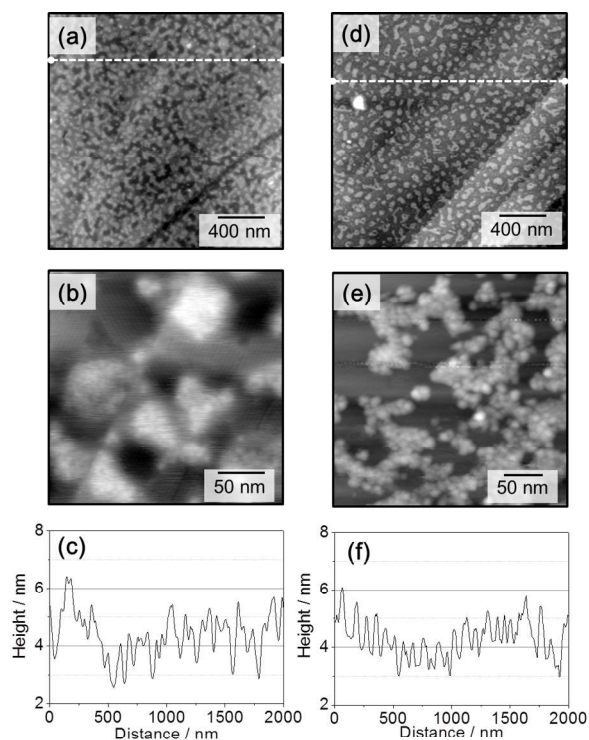


Fig. 2 (a), (b) AFM images of HOPG surface after deposition of PtNPs by spin coating (thin PtNPs/HOPG, $2 \times 2 \mu\text{m}$ for (a) and $200 \times 200 \text{ nm}$ for (b)). (c) Cross-sectional profile along the dashed line shown in (a). (d), (e) AFM images of the Pt NPs after ORC ($2 \times 2 \mu\text{m}$ for (a) and $200 \times 200 \text{ nm}$ for (b)). (f) Cross-sectional profile along the dashed line shown in (d). were present in an island structure. The typical height of a PtNP island estimated by AFM was 2 nm (Fig. 2c), which is in good agreement with the diameter of the as-syn. PtNPs estimated from TEM images ($d = 1.6 \pm 0.6 \text{ nm}$). Thus, the PtNPs in the thin

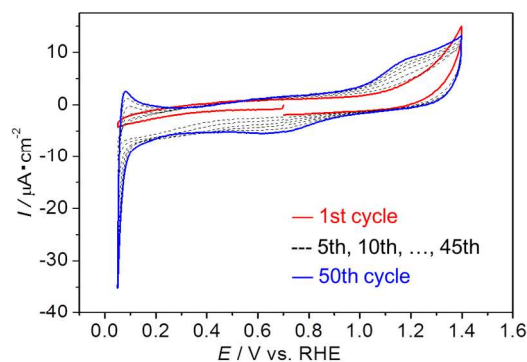


Fig. 3 Cyclic voltammograms of thin PtNPs/HOPG during ORC treatment. Red line: 1st cycle. Dotted lines: every fifth cycle. Blue line: stable CV after the 50th cycle. Electrolyte = 0.1 M HClO₄. Scan rate = 0.05 V s⁻¹.

PtNPs/HOPG were almost dispersed as a monolayer on the HOPG surface.

Electrochemical measurements were performed in 0.1 M HClO₄ aqueous solution. Fig. 3 shows cyclic voltammograms (CVs) with multiple ORC from 0.05 to 1.45 V vs. RHE. In the first cycle, little current was observed because of the presence of dodecanethiol on the surface of the PtNPs. The electrocatalytic activity of PtNPs for the HER around 0.05 V increased as potential scans were repeated. The Pt/PtO redox couple was observed at $E_{\text{pa}} = 1.16 \text{ V}$ and $E_{\text{pc}} = 0.68 \text{ V}$ and increased in height with increasing number of potential cycles. At the oxidative potential the dodecanethiol layers coated on the PtNP surface were removed and at the reduction potential Pt metal surface was exposed and activated for the HER. After fifty scans, CVs were stabilized. The cathodic charge between 0.35 to 0.07 V of stable CVs (Fig. 3, blue) was integrated and used for platinum surface area estimation. From the result, the electrochemically effective Pt surface area was 5% of the surface area of HOPG.

After ORC treatment, the surface morphology of HOPG was again examined by AFM (Fig. 2d). PtNPs maintained their island-like morphology on the HOPG surface to form a thin layer with a height of 2 nm. A high-resolution AFM image (Fig. 2e) showed the island was composed of nanoparticles with an average diameter of 2 nm on the surface of HOPG. From the electrochemical measurements, EXAFS and AFM results, the estimated loading density of Pt atoms was about $1 \times 10^{14} \text{ atom}\cdot\text{cm}^{-2}$. The estimation detail is described in Supplementary Information. Note that the careful electrochemical treatment prevented the activated Pt nanoparticles from aggregating to form large particles. This might be because the applied positive potential was less than the bulk oxidation of Pt and sufficient for the oxidation of thiols, so Pt was not ionized and was not dissolved into the solution. Furthermore, PtNPs could not migrate collectively on the HOPG surface during the mild CV processes.

XAFS Measurement in Air

Fig. 4(i) shows the transmission XAFS oscillation of as-syn. PtNPs dissolved in solution. Pt-Pt oscillation was observed up to 140 nm⁻¹ with an average bond distance of $0.274 \pm 0.001 \text{ nm}$ (See Supplementary Information). Compared to Pt foil and PtO₂, the thin PtNPs on HOPG was maintained their metallic state, as shown in Fig. 5.

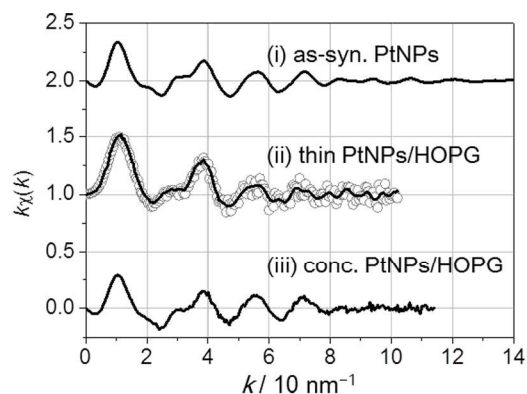


Fig. 4 Extracted XAFS oscillation, $k\chi(k)$. (i) As synthesized PtNP solution in transmission mode. (ii) 1×10^{14} Pt atoms \cdot cm $^{-2}$ thin PtNPs/HOPG obtained with back-side illumination (BI) configuration. Bold line shows the smoothing of a five-point average. (iii) Concentrated PtNPs/HOPG measured with a BI configuration.

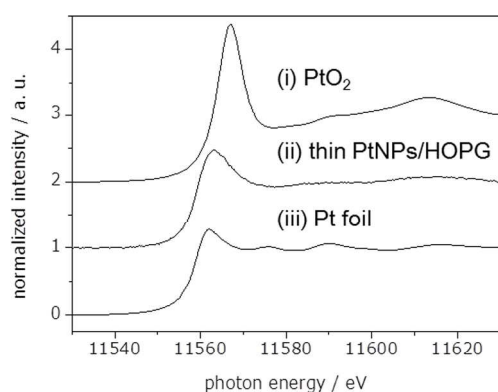


Fig. 5 XANES spectra of (i) PtO $_2$, (ii) thin PtNPs/HOPG and (iii) Pt foil. Thin PtNPs /HOPG was measured in air in a BI-FXAFS mode without BCLA.

To compare the BI-FXAFS and PTRF-XAFS measurements, a PtNP sample of higher concentration was required for BI-FXAFS because we could not obtain a clear L $_3$ edge in the sample with 10^{14} Pt atoms \cdot cm $^{-2}$ on HOPG. A sample with 10^{16} Pt atoms \cdot cm $^{-2}$ was deposited on HOPG so the surface was fully covered with a multilayer of PtNPs (denoted conc. PtNPs/HOPG), as observed by AFM (Fig. S3 in Supplementary Information). Fig. 6(i) shows a PTRF-XAFS spectrum measured in air without ORC treatment. We found an edge jump followed by a distorted post-edge background with little XAFS oscillation observed. The pre-edge also showed a curious shape. Total reflection occurred when the X-ray was set at a grazing angle, but the cut-off angle could not be sharply defined. On typical single-crystal metal or oxide surfaces, total reflection occurs only to the specular direction with the reflected beam appearing as a sharp spot. On the HOPG surface, a reflection band appeared between the specular direction and direct beam in a photograph set 0.8 m behind the sample. The HOPG sample contained wrinkles, where atomically flat HOPG surfaces are oriented randomly, so total reflection conditions were not always satisfied. Fig. 6(ii) shows the XAFS spectrum for conc. PtNPs/HOPG in air using a BI configuration. A much clearer XAFS spectrum was obtained. The XAFS oscillation was extracted, and is shown in Fig. 4(iii). Fig. 4(ii) shows the XAFS

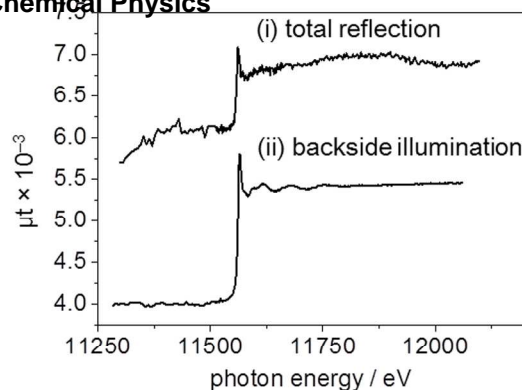


Fig. 6 EXAFS spectra of conc. PtNP layers measured at an air/HOPG interface. (i) Total reflection configuration. (ii) BI configuration.

oscillations for the thin Pt NPs / HOPG. Even with such a small amount of PtNPs, we could observe XAFS oscillations up to 70 nm $^{-1}$ in k -space. The XAFS oscillation is similar to that observed in solution, indicating the presence of PtNPs. Thus, BI-FXAFS using a thin HOPG window can detect the structure of PtNPs on an HOPG substrate in air.

30 XAFS Measurements at an Electrolyte/HOPG Interface

The scattering from air was very small. However, when electrolyte was present, the background scattering became larger because of the coexisting electrolyte. Fig. 7(a) shows the fluorescence signal in the Pt L $_3$ edge XANES region of thin PtNPs/HOPG using the BI method in the presence of 0.1 M HClO $_4$ solution. The difference between Fig. 4(ii) and Fig. 7(a) was only the environment; *i.e.*, in air or in solution. We observed large elastic scattering from solution. The Ge filter and Soller slits³⁹ positioned before the 19-element SSD were ineffective and the tail of the elastic scattering completely hid the fluorescence X-ray signal. The absorption edge was hardly observed, as illustrated in Fig. 7(a). When a BCLA was inserted before the 19-element pure Ge detector, we could observe the edge jump. Fig. 7(b)-(i) and (ii) show the fluorescence XAFS spectra obtained in air and water, respectively. The background X-ray was remarkably decreased when using the BCLA, so that spectra with a better S/B ratio were obtained. However, the count rate was quite low, *ca.* 1/1000 of the fluorescence without the BCLA because of the low throughput of BCLA (as shown in supplementary information). The BCLA improved the detection limit and we could measure a fluorescence XAFS signal from Pt on the thin HOPG window even in the presence of water. Since the fluorescent X-ray signals through BCLA were small, we did not carry out the EXAFS measurement due to the limited beam time.

Fig. 8 shows the XANES spectra of thin PtNPs/ HOPG obtained at $E = 0.35$ and 0.15 V vs. RHE after the dodecanethiol layer was removed by ORC. The incident angle was set at about 50 $^\circ$ (nearly the magic angle). Note that no major difference was observed in the XANES region between before (shown in Fig. 7) and after removal of the dodecanethiol layer (shown in Fig. 8 (a)). When the electrode potential was set at $E = 0.15$ V, the white line was slightly modified. A difference spectrum revealed a new structure. Although the spectra were rather noisy, we carried out the F-test (see supplementary information) and found the peak around 11559 eV was meaningful with the confidence level more than 0.8. Kubota *et al.*^{40, 41} reported that adsorbed hydrogen induced the modification of the white line. They showed the

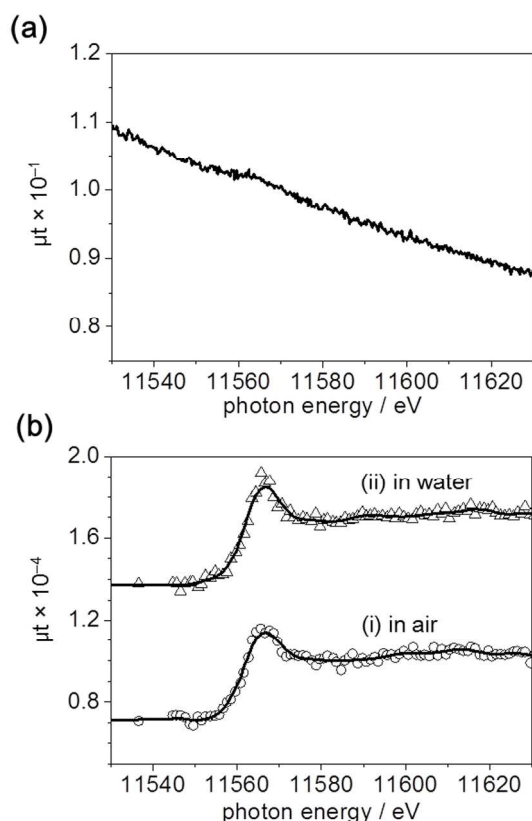


Fig. 7 (a) XANES spectrum of thin PtNPs/HOPG at Pt L_3 edge contact with 0.1 M HClO_4 electrolyte solution and a Ge filter. (b) XANES spectra obtained with BCLA in (i) air and (ii) electrolyte solution. Bold line shows the smoothing of a five-point average.

difference spectrum well corresponding to the one observed in this study. It has been demonstrated that the modification of this peak is related to the multiple scattering of photoelectrons induced by hydrogen.^{42,43} At this potential, adsorption of hydrogen was expected from the CV measurements. The protons were reduced to hydrogen and hydrogen was adsorbed onto the clean Pt electrode at the positive potential with respect to RHE, so-called underpotential deposition conditions.⁴⁴⁻⁴⁶

We changed the incident X-ray angles at $E = 0.35$ V to observe the effect on structure and electronic state, as shown in Fig. 8(b). An angle of 50° is close to the magic angle, so the signal is less polarization dependent. In contrast, an incident angle of 15° provides more information about the structure parallel to the surface normal direction.¹⁹ When the incident X-ray was 15° to the substrate, the white-line intensity was stronger than that at 70° . The white-line intensity depends on the density of empty d states, indicating that more empty states are produced by the adsorption of oxygen in the normal direction to the HOPG surface. We could obtain information about anisotropic adsorption of PtNPs by polarization-dependent XANES measurements, although the origin of such anisotropic adsorption is unknown.

Conclusions

Polarization-dependent XAFS was obtained from model PtNPs deposited on HOPG surfaces using BI and BCLA to select only

the Pt L_{α} fluorescence. In air, we obtained successful measurements only using the developed BI method. However, in the presence of water, we had to use a BCLA to reduce scattering to measure Pt L_3 edge XAFS. This configuration allowed us to obtain potential- and polarization-dependence measurements. Further investigation on PtNPs/HOPG under a high-brilliance undulator beam line and improvement of the throughput of the BCLA are currently in progress.

Acknowledgement

This work was carried out with the approval of the Photon Factory Advisory Committee (PAC Nos. 2010G601 and 2012G094), and was financially supported by the New Energy and Industrial Technology Development Organization (NEDO).

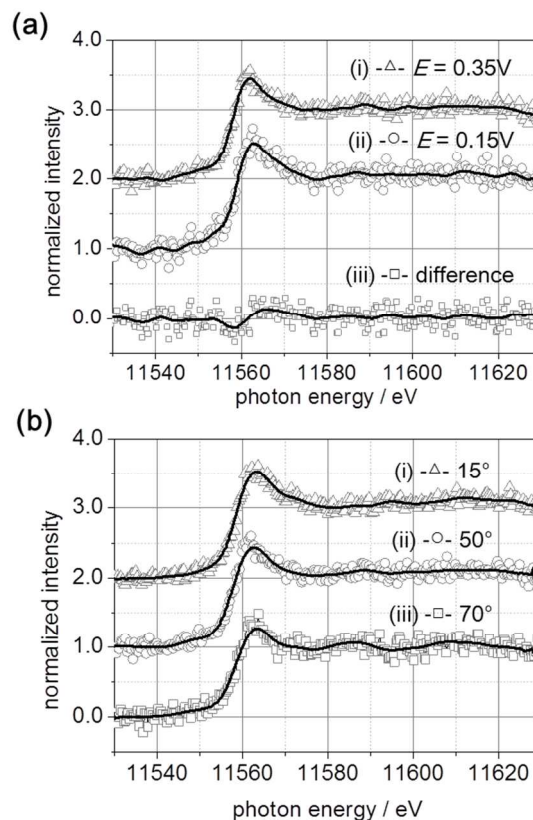


Fig. 8 (a) Normalized XANES spectrum of thin PtNPs/HOPG after ORC treatment. An offset of 1.0 is applied to the data (i) for clarity. Difference spectrum, [(ii)-(i)] and smoothing line are shown. (b) Polarization-dependent XANES spectra obtained at $E = 0.35$ V.

Notes and references

^a Catalysis Research Center, Hokkaido University, Sapporo, Hokkaido 001-0021, Japan. E-mail: askr@cat.hokudai.ac.jp;

Fax: +81-11-706-9113; Tel: +81-11-706-9113

^b Photon Factory, Institute of Materials Structure Science, High-Energy Accelerator Research Organization, Tsukuba, Ibaraki 305-0801, Japan.

^c Department of Engineering Science, the University of Electro-Communications. Chofu, Tokyo 182-8585, Japan.

1. R. Subbaraman, D. Strmcnik, V. Stamenkovic and N. M. Markovic, *J Phys Chem C*, 2010, **114**, 8414-8422.

2. Y. M. Maksimov, B. I. Podlovchenko and T. L. Azarchenko, *Electrochim Acta*, 1998, **43**, 1053-1059.
3. Y. Ayato, K. Kunimatsu, M. Osawa and T. Okada, *J Electrochem Soc*, 2006, **153**, A203-A209.
4. A. M. Gomez-Marin, A. Berna and J. M. Feliu, *J Phys Chem C*, 2010, **114**, 20130-20140.
5. T. Kondo, T. Suzuki and J. Nakamura, *J Phys Chem Lett*, 2011, **2**, 577-580.
6. M. Bayati, J. M. Abad, R. J. Nichols and D. J. Schiffrin, *J Phys Chem C*, 2010, **114**, 18439-18448.
7. Y. K. Zhou, R. Pasquarelli, T. Holme, J. Berry, D. Ginley and R. O'Hayre, *J Mater Chem*, 2009, **19**, 7830-7838.
8. K. Yasuda, A. Taniguchi, T. Akita, T. Ioroi and Z. Siroma, *Phys Chem Chem Phys*, 2006, **8**, 746-752.
9. Y. Y. Shao, G. P. Yin, Y. Z. Gao and P. F. Shi, *J Electrochem Soc*, 2006, **153**, A1093-A1097.
10. P. J. Ferreira, G. J. la O', Y. Shao-Horn, D. Morgan, R. Makharia, S. Kocha and H. A. Gasteiger, *J Electrochem Soc*, 2005, **152**, A2256-A2271.
11. V. O. Mittal, H. R. Kunz and J. M. Fenton, *J Electrochem Soc*, 2006, **153**, A1755-A1759.
12. A. Taniguchi, T. Akita, K. Yasuda and Y. Miyazaki, *J Power Sources*, 2004, **130**, 42-49.
13. T. Akita, A. Taniguchi, J. Maekawa, Z. Siroma, K. Tanaka, M. Kohyama and K. Yasuda, *J Power Sources*, 2006, **159**, 461-467.
14. M. Cai, M. S. Ruthkosky, B. Merzougui, S. Swathirajan, M. P. Balogh and S. H. Oh, *J Power Sources*, 2006, **160**, 977-986.
15. Y. H. Zhang, M. L. Toebes, A. van der Eerden, W. E. O'Grady, K. P. de Jong and D. C. Koningsberger, *J Phys Chem B*, 2004, **108**, 18509-18519.
16. T. Saida, O. Sekizawa, N. Ishiguro, M. Hoshino, K. Uesugi, T. Uruga, S.-i. Ohkoshi, T. Yokoyama and M. Tada, *Angewandte Chemie*, 2012, **124**, 10457-10460.
17. M. Tada, S. Murata, T. Asakoka, K. Hiroshima, K. Okumura, H. Tanida, T. Uruga, H. Nakanishi, S. Matsumoto, Y. Inada, M. Nomura and Y. Iwasawa, *Angew Chem Int Edit*, 2007, **46**, 4310-4315.
18. N. Ishiguro, T. Saida, T. Uruga, S. Nagamatsu, O. Sekizawa, K. Nitta, T. Yamamoto, S. Ohkoshi, Y. Iwasawa, T. Yokoyama and M. Tada, *Acc Catal*, 2012, **2**, 1319-1330.
19. K. Asakura, in *Catalysis*, RSC publishing, Editon edn., 2012, vol. 24, pp. 281-322.
20. Y. Koike, K. Ijima, W. J. Chun, H. Ashima, T. Yamamoto, K. Fujikawa, S. Suzuki, Y. Iwasawa, M. Nomura and K. Asakura, *Chem Phys Lett*, 2006, **421**, 27-30.
21. K. Tamura, H. Oyanagi, T. Kondo, M. Koinuma and K. Uosaki, *J Phys Chem B*, 2000, **104**, 9017-9024.
22. D. Takamatsu, Y. Koyama, Y. Orikasa, S. Mori, T. Nakatsutsumi, T. Hirano, H. Tanida, H. Arai, Y. Uchimoto and Z. Ogumi, *Angew Chem Int Edit*, 2012, **51**, 11597-11601.
23. A. Balut, J. Robinson, K. J. Roberts, M. E. Herron and F. C. Walsh, *Jpn J Appl Phys* 1, 1993, **32**, 422-424.
24. T. P. Trainor, A. S. Templeton and P. J. Eng, *J Electron Spectrosc*, 2006, **150**, 66-85.
25. H. Prinz and H. H. Strehblow, *Electrochim Acta*, 2002, **47**, 3093-3104.
26. T. Masuda, H. Fukumitsu, K. Fugane, H. Togasaki, D. Matsumura, K. Tamura, Y. Nishihata, H. Yoshikawa, K. Kobayashi, T. Mori and K. Uosaki, *J Phys Chem C*, 2012, **116**, 10098-10102.
27. C. Lee, X. D. Wei, J. W. Kysar and J. Hone, *Science*, 2008, **321**, 385-388.
28. K. S. Novoselov, A. K. Geim, S. V. Morozov, D. Jiang, Y. Zhang, S. V. Dubonos, I. V. Grigorieva and A. A. Firsov, *Science*, 2004, **306**, 666-669.
29. Y. Gorlin, B. Lassalle-Kaiser, J. D. Benck, S. Gul, S. M. Webb, V. K. Yachandra, J. Yano and T. F. Jaramillo, *Journal of the American Chemical Society*, 2013, **135**, 8525-8534.
30. H. Niwa, H. Kiuchi, J. Miyawaki, Y. Harada, M. Oshima, Y. Nabae and T. Aoki, *Electrochem Commun*, 2013, **35**, 57-60.
31. A. Kolmakov, D. A. Dikin, L. J. Cote, J. X. Huang, M. K. Abyaneh, M. Amati, L. Gregoratti, S. Gunther and M. Kiskinova, *Nat Nanotechnol*, 2011, **6**, 651-657.
32. T. Masuda, H. Yoshikawa, H. Noguchi, T. Kawasaki, M. Kobata, K. Kobayashi and K. Uosaki, *Appl Phys Lett*, 2013, **103**.
33. C. Karanfil, G. Bunker, M. Newville, C. U. Segre and D. Chapman, *J Synchrotron Radiat*, 2012, **19**, 375-380.
34. Z. Zhong, D. Chapman, B. Bunker, G. Bunker, R. Fischetti and C. Segre, *J Synchrotron Radiat*, 1999, **6**, 212-214.
35. A. J. Kropf, R. J. Finch, J. A. Fortner, S. Aase, C. Karanfil, C. U. Segre, J. Terry, G. Bunker and L. D. Chapman, *Rev Sci Instrum*, 2003, **74**, 4696-4702.
36. C. Dablemont, P. Lang, C. Mangeney, J. Y. Piquemal, V. Petkov, F. Herbst and G. Viau, *Langmuir*, 2008, **24**, 5832-5841.
37. K. Asakura, ed. Y. Iwasawa, World Scientific, Editon edn., 1996, vol. 2, pp. 33-58.
38. T. Taguchi, T. Ozawa and H. Yashiro, *Physica Scripta* 2005, **T115**, 205.
39. F. W. Lytle, R. B. Greigor, D. R. Sandstrom, E. C. Marques, J. Wong, C. L. Spiro, G. P. Huffman and F. E. Huggins, *Nucl Instrum Meth A*, 1984, **226**, 542-548.
40. K. Asakura, T. Kubota, N. Ichikuni and Y. Iwasawa, *Stud. Surf.Sci.Catal.* (Proc.11th Int. Congr. on Catal.), Baltimore, USA, 1996.
41. T. Kubota, K. Asakura, N. Ichikuni and Y. Iwasawa, *Chem Phys Lett*, 1996, **256**, 445-448.
42. K. Ohtani, T. Fujikawa, T. Kubota, K. Asakura and Y. Iwasawa, *Japanese Journal of Applied Physics Part 1-Regular Papers Brief Communications & Review Papers*, 1997, **36**, 6504-6510.
43. A. L. Ankudinov, J. J. Rehr, J. Low and S. R. Bare, *Phys Rev Lett*, 2001, **86**, 1642-1645.
44. S. Mukerjee and J. McBreen, *J Electroanal Chem*, 1998, **448**, 163-171.
45. S. Mukerjee, S. Srinivasan, M. P. Soriaga and J. McBreen, *J Electrochem Soc*, 1995, **142**, 1409-1422.
46. M. Teliska, V. S. Murthi, S. Mukerjee and D. E. Ramaker, *J Electrochem Soc*, 2005, **152**, A2159-A2169.